Astroparticle Physics 66 (2015) 53–60

Contents lists available at ScienceDirect

Astroparticle Physics

journal homepage: www.elsevier.com/locate/astropart

A study of the trace ^{39}Ar content in argon from deep underground sources

J. Xu [a,*], F. Calaprice [a], C. Galbiati [a], A. Goretti [a], G. Guray [a], T. Hohman [a,1], D. Holtz [a,2], An. Ianni [a], M. Laubenstein [b], B. Loer [a,3], C. Love [c,4], C.J. Martoff [c], D. Montanari [a,3], S. Mukhopadhyay [d], A. Nelson [a], S.D. Rountree [e], R.B. Vogelaar [e], A. Wright [a,5]

[a] Department of Physics, Princeton University, Princeton NJ 08544, USA
[b] INFN Laboratori Nazionali del Gran Sasso, SS 17 bis Km 18_910, 067010 Assergi (AQ), Italy
[c] Physics Department, Temple University, Philadelphia, PA 19122, USA
[d] Department of Earth and Planetary Sciences, Harvard University, Cambridge, MA 02138, USA
[e] Physics Department, Virginia Polytechnic Institute and State University, Blacksburg, VA 24061, USA

ARTICLE INFO

Article history:
Received 6 April 2014
Received in revised form 8 December 2014
Accepted 12 January 2015
Available online 19 January 2015

Keywords:
Underground argon
^{39}Ar
Dark matter instrumentation
Low-radioactivity technique
Low-background counting

ABSTRACT

The discovery of argon from deep underground sources with significantly less ^{39}Ar than atmospheric argon was an important step in the development of direct dark matter detection experiments using argon as the active target. We report on the design and operation of a low-background single-phase liquid argon detector that was built to study the ^{39}Ar content of this underground argon. Underground argon from the Kinder Morgan CO_2 plant in Cortez, Colorado was determined to have less than 0.65% of the ^{39}Ar activity in atmospheric argon, or 6.6 mBq/kg specific ^{39}Ar activity.

1. Introduction

Argon has been considered as an excellent medium in the direct detection of Weakly Interacting Massive Particles (WIMPs). Argon-based scintillation detectors can make use of pulse shape discrimination (PSD) to separate WIMP-induced nuclear recoil signals from electron recoil backgrounds with extremely high efficiency ($\sim 10^8$, with potential improvement to 10^{10}) [1–3]. Argon-based detectors can also be operated as ionization detectors, or as two-phase scintillation–ionization Time Projection Chambers (TPCs) [4] that have even more background suppression capability.

Argon-based WIMP dark matter searches, however, must confront the presence of intrinsic ^{39}Ar, a beta emitter with an endpoint energy of 565 keV and half-life of 269 years. ^{39}Ar is present at an activity of $\sim$1 Bq/kg in atmospheric argon [5]. Even with PSD, the ^{39}Ar activity in atmospheric argon limits the ultimate size of argon-based experiments and restricts their ability to probe very low energy events.

The ^{39}Ar activity in the atmosphere is mainly produced and maintained by cosmic ray induced nuclear reactions such as ^{40}Ar(n,2n)^{39}Ar. Because of the long lifetime of ^{39}Ar, the only practical way to reduce the amount of ^{39}Ar in atmospheric argon is isotope separation. This is possible, but costly and time consuming for ton-scale argon detectors.

Most of the ^{40}Ar in the atmosphere was produced by electron capture decays of long-lived ^{40}K within the Earth and much of the ^{40}Ar produced remains underground. It might be expected that argon from underground sources would have less ^{39}Ar radioactivity since cosmic rays can be efficiently attenuated by rocks. Unfortunately, as shown in studies by Loosli, Lehmann and Balderer [6] and Lehmann [7], ^{39}Ar can be produced underground by the (n,p) reaction of radiogenic neutrons on stable potassium, ^{39}K$(n,p)^{39}$Ar. The average ^{39}Ar concentration in crustal argon is

* Corresponding author.
E-mail address: jingkexu@princeton.edu (J. Xu).
[1] Current address: Department of Mechanical and Aerospace Engineering, Princeton University, Princeton NJ 08544, USA.
[2] Current address: Department of Physics and Astronomy, The Johns Hopkins University, Baltimore, MD 21218, USA.
[3] Current address: Fermi National Accelerator Laboratory, Batavia, IL 60510, USA.
[4] Formerly C. Martin.
[5] Current address: Department of Physics, Queen's University, Kingston, ON, K7L 3N6, Canada.

http://dx.doi.org/10.1016/j.astropartphys.2015.01.002
0927-6505/

not expected to be significantly lower than that in atmospheric argon. However, because the uranium and thorium content of rocks, which determines the local radiogenic neutron flux, varies in the crust, the ^{39}Ar concentration in underground argon vary from place to place, with measured ^{39}Ar levels ranging from 20 times lower to 16 times higher than the atmospheric value [7,8].

A search was undertaken by the Princeton group for a large supply of underground argon low in ^{39}Ar. An early promising measurement was made on argon that was extracted from the crude helium in the National Helium Reserve [9]. The ^{39}Ar content in this argon was measured to be less than 5% of the level in atmospheric argon, using a low background gas counter in the laboratory of H. H. Loosli in Bern, Switzerland. However, large scale argon extraction from the National Helium Reserve was found to be impractical.

Compared to the Earth's crust, which has uranium and thorium at ppm levels, the Earth's mantle is thought to contain these elements at the ppb level [10]. Thus, the ^{39}Ar content in mantle argon could be a few orders of magnitude lower than that in crustal argon. Measurements of isotope abundances in the rare gases (helium, neon, argon, krypton, and xenon) derived from CO_2 gas wells in the U.S. Southwest indicate that these gases originate in the Earth's upper mantle [11–13], and thus these wells should be a good source of argon low in ^{39}Ar. The crude gas from the National Helium Reserve, on the contrary, was extracted from natural gas and is believed to have a crust origin.

The argon gas extraction system used at the National Helium Reserve was upgraded to increase its capacity, and deployed at the Reliant Dry Ice facility on the Bravo Dome CO_2 gas field in Bueyeros, New Mexico. First samples showed no sign of ^{39}Ar, but later measurements yielded evidence for ^{39}Ar contamination, possibly due to a decrease in well pressure as the CO_2 was consumed. The gas collection system was further upgraded and moved to the Kinder Morgan CO_2 well in Cortez, Colorado. We are currently extracting argon at this site at a rate of a few hundred grams per day [14]. At the time of this writing, approximately 160 kg of underground argon has been collected. The results presented in this work are based on kg-sized samples of argon collected at Cortez in 2009 and 2011, which will be referred to as the first sample and the second sample respectively in the discussions.

In this paper we describe a custom low-background liquid argon detector that was designed to improve the sensitivity and the robustness of the ^{39}Ar measurement as compared to that in reference [9]. The detector is described in Section 3. Using this approach, we obtained in 2011 a new, more stringent upper limit of 0.65% on the ^{39}Ar abundance in the first argon sample extracted from the Cortez site, relative to atmospheric argon (see Section 4). This result demonstrates the highest sensitivity to ^{39}Ar in argon of all known techniques [9,15–17]. A follow-up measurement made in 2012 using the second underground argon sample obtained similar results (see Section 5), indicating that the ^{39}Ar content in these wells has remained low. These limits for ^{39}Ar demonstrate that experiments using underground argon active volumes will significantly outperform those with atmospheric argon, especially in their sensitivity to low mass WIMPs. Moreover, even at the current upper limit of ^{39}Ar, dark matter searches using multi-ton scale argon detectors are practical with underground argon. The DarkSide-50 detector has been launched with the intention of using underground argon along with other innovative technologies for a sensitive dark matter search; it will also demonstrate near background-free operation in multi-ton argon detectors [18]. Detailed discussion on this work and its implications can be found in the Ph.D thesis [19].

2. Purification of underground argon

As described in Ref. [14], the raw carbon dioxide gas at the Cortez site is processed by a vacuum-pressure-swing adsorption (VPSA) unit that produces a crude mixture of approximately 40% nitrogen, 55% helium, and 5% argon by volume. A cryogenic distillation column was later constructed at FNAL to further purify the crude argon gas, which produced argon of >99.9% purity [20]. This system was used to provided the second underground argon sample for the 2012 measurement reported in this paper.

The first underground argon sample was collected before the distillation column existed, and it was purified at Princeton University using a zeolite column. The column contained 18 kg of Zeochem's Zeox Z12–07 zeolite in a 30 L aluminum gas cylinder, which absorbed the nitrogen content in the gas mixture and produced an effluent stream of concentrated argon and helium. This remaining gas was then passed through a 6L charcoal trap consisting of 2 kg of activated OVC 4x8 charcoal in a stainless-steel bottle immersed in liquid nitrogen. This cryogenic charcoal trap captured the argon while allowing the helium to escape. The product argon gas has a nitrogen concentration less than 1% by volume, and it has been demonstrated that further iterations of this process can bring the nitrogen level below 0.1% [19].

Both of the underground argon samples were further treated using hot calcium to remove the remaining impurities. A calcium trap, illustrated in Fig. 1, held trays that were filled with granules of >98.0% purity calcium within a Conflat-sealed stainless-steel cylinder. The calcium was heated above its melting point (842 °C) for a short time, then the temperature was reduced slightly for the gettering action. The argon-rich gas was fed over the hot calcium at ~1 L/min, allowing the calcium to react with the impurities in the stream. The stable solids produced by these reactions, including calcium nitride, remained in the trays, while argon, as a noble gas, passed through the trap and was collected in a cryogenic charcoal trap. The calcium trap could be refreshed by heating it above the melting point to expose a fresh layer of calcium; this cycle could be repeated until the calcium was largely consumed. Then the trap was opened, cleaned, and reloaded with fresh calcium. The calcium trap was also used in the inline purification as the argon gas was being filled into the detector for ^{39}Ar measurements.

The first underground argon sample had been stored in a Princeton laboratory with little overburden before the measurement in 2011. The surface storage of about three years is ~1% of the ^{39}Ar half life. Considering the equilibrium between ^{39}Ar decay and ^{39}Ar production in the atmosphere, the generation of ^{39}Ar in the sample during the storage period is a potential concern. However, the cosmogenic neutron flux at the Earth's surface is a few orders of magnitude lower than the average value in the atmosphere [21],

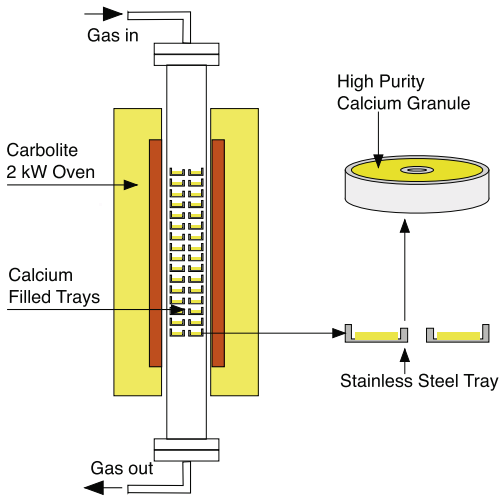

Fig. 1. The calcium trap used for argon purification.

suggesting that ^{39}Ar production at surface should be suppressed by a similar factor. A calculation using the COSMO code [22] confirmed that the equilibrium ^{39}Ar activity in argon stored on surface is only 1.7 mBq/kg, so after three years of surface exposure the activity will be $\ll$1.7 mBq/kg, which would not be a concern to the experiment.

3. Apparatus

The low background detector, as configured for the measurement of the first underground argon sample reported here, is illustrated in Fig. 2. It contained 0.56 kg of liquid argon as the active volume in a 2.5-inch inner diameter, 5.25-inch high "cup" made of highly crystalline PTFE. The inner surfaces of the PTFE container and the fused silica top window were coated with ~300 μg/cm^2 of p-Terphenyl [23,24] via vacuum evaporation to shift the 128 nm ultraviolet argon scintillation light into the visible range. The photons were detected by a low background, high quantum efficiency(>30%), 3-inch, Hamamatsu R11065 cryogenic photomultiplier tube (PMT) above the cup. The cup and PMT were enclosed within a 3.5-inch diameter copper and stainless steel sleeve, which was sealed at the top by a Conflat flange. The side and bottom of the sleeve were surrounded by 2 inches of oxygen-free high conductivity (OFHC) copper shielding; a loose-fitting 2.5-inch thick copper plug was inserted into the sleeve above the PMT to complete the inner shielding.

The inner detector and the copper shielding around it were cooled by a bath of commercial liquid argon in an open cryostat. The liquid level in the cooling bath was maintained by a model LC10 Teragon Research liquid level controller attached to a low pressure liquid argon supply dewar. The open cryostat sat within, and was supported by, a lead castle that was 8 inches thick on the sides, 12 inches thick on the bottom, and 4 inches thick on the top. A muon veto system, composed of 2 inches thick plastic scintillator panels, covered the sides and top of the lead.

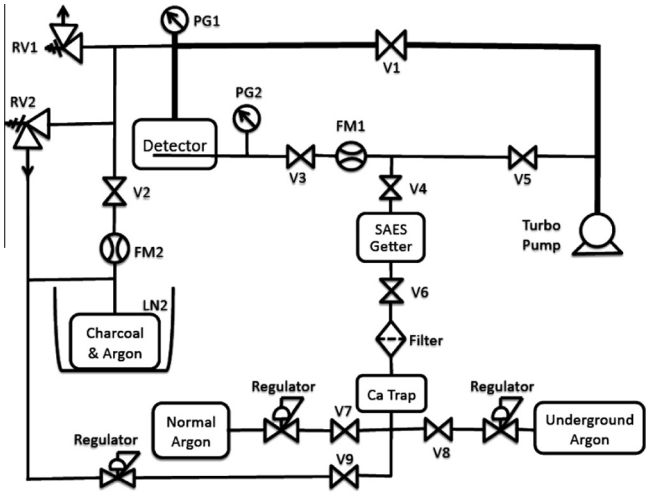

Fig. 3. The gas handling system for the low background argon detector. The underground argon could be purified as the detector was filled, and fully recovered without loss with the liquid nitrogen cooled charcoal trap.

The components of the low background detector gas handling system, shown in Fig. 3, were connected with copper tubing and Swagelok fittings. The gas plumbing and the detector could be evacuated using a turbo-molecular pump (Pfeiffer Vacuum HiCube), with typical vacuum levels of 10^{-6} mbar achieved. When the detector was being filled, the argon gas was purified using both the calcium trap described earlier and a Mono-Torr zirconium getter to remove impurities such as water, oxygen, and nitrogen before being condensed in the pre-cooled detector volume. To empty the detector, cooling was stopped and as the underground argon evaporated it was recovered by condensing it in a charcoal-filled aluminum gas cylinder partially immersed in a bath of

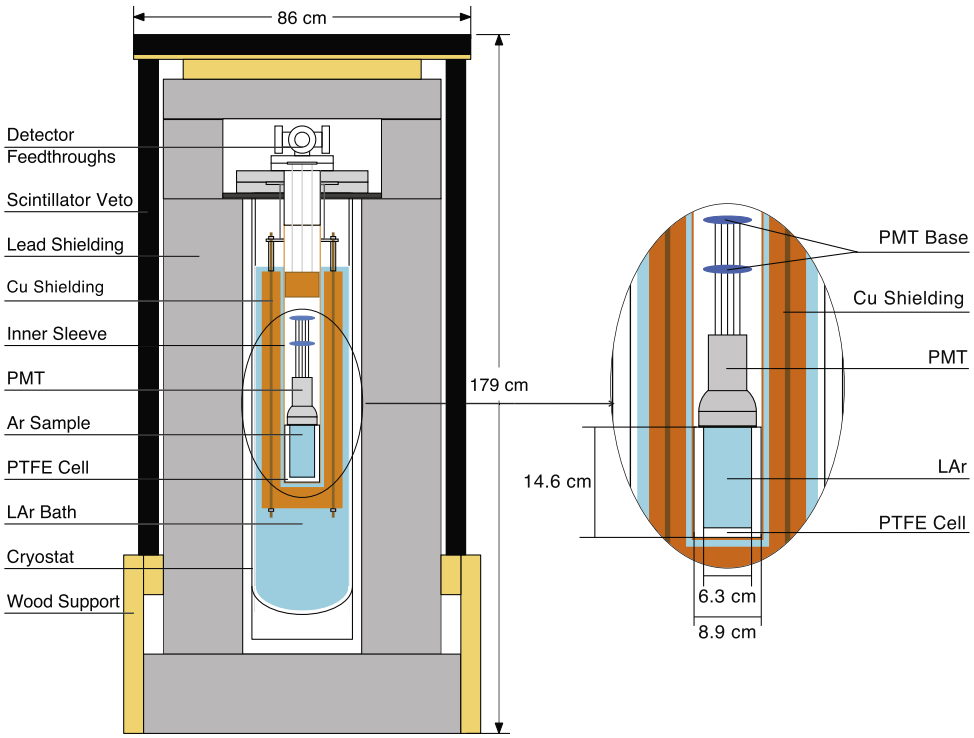

Fig. 2. A schematic diagram of the low background detector. The active volume of liquid argon is surrounded by a PTFE cell coated with WLS, and viewed by a low background PMT. Copper and lead shielding reduce external backgrounds. An external liquid argon bath provides cooling for the inner detector.

liquid nitrogen. The use of LN_2-cooled activated charcoal allowed for transfer and recovery of the argon without the use of mechanical compressors that could introduce impurities.

Data acquisition was carried out using 12 bit, 250 MHz digitizers (CAEN V1720). The output of the inner detector PMT was digitized directly. The signals from the ten PMTs of the muon veto system were processed by LeCroy 623B amplitude discriminators, the output of which was logically summed and fed into a second digitizer channel. Readout of both digitizer channels was triggered by an amplitude discriminator on the inner PMT channel. For each event, 15 μs of data were recorded, beginning 5 μs before the trigger.

4. Measurement of the first underground argon sample

The detector was commissioned in a ground-level laboratory at Princeton University, and later relocated underground at a depth of ~1450 meter water equivalent (m.w.e.) in the Kimballton Underground Research Facility (KURF) in Virginia. In each measurement campaign, the detector was operated with samples of atmospheric and underground argon. The data presented here were obtained in 2011.

4.1. Data processing

The energy response of the detector was monitored using a 10 μCi ^{137}Cs source that could be introduced between the lead shielding and the cryostat containing the liquid argon bath. As shown in Fig. 4, the relative light yield decreased slowly with time (~0.6% per day) as impurities released from inner detector components accumulated. Given the relatively short duration of each measurement (typically one week), it was efficient to monitor and correct the drift in the light yield with calibration data, instead of implementing an in-run purification system.

After the energy scale of both atmospheric argon data and underground argon data was corrected to produce matching ^{137}Cs spectra, the underground argon spectrum was subtracted from the atmospheric argon spectrum and the resulting ^{39}Ar spectrum was fitted to the theoretical one with energy resolution applied. This fit provided the absolute energy scale of the detector, which correctly included the spatial variation of light collection efficiency in the sensitive volume.[6] Throughout this paper, energy is given in keV_{ee} (electron equivalent energy), assuming a linear scintillation response scaled from the ^{39}Ar calibration data. While quenching occurs for nuclear recoil events and low energy electron recoil events [25], the linearity assumption holds well for the particles and energy range of interest for this analysis.

The light yield of the detector was evaluated by using the single photoelectron (p.e.) pulses as a reference. In the runs at Princeton, typical light yields of 6–7 p.e./keV_{ee} were observed at a slow component lifetime of 1.45–1.55μs (corrections from relaxation of slow argon scintillation were not applied). The uncorrected light yield in the KURF measurement was lower, at ~5 p.e./keV_{ee} with a lifetime ~1.3 μs.

The time profile of liquid argon scintillation pulses depends strongly on the density of ionization produced by the exciting particle, and thus the pulse shape of the scintillation signal can be used to distinguish electron recoil events and nuclear recoil events with very high efficiency. As shown in Fig. 5, the F_{prompt} parameter, defined as the fraction of light in an argon scintillation pulse that arrives within the first 90 ns, is distinctly different in electron recoil events and nuclear recoil events. A cut on F_{prompt} was used to select the electron recoil events for the ^{39}Ar analysis, which was the only explicit cut applied to the data at KURF. The data acceptance in the F_{prompt} region from 0.05 to 0.55 was greater than 99% for energies above 50 keV_{ee}, with a very high rejection efficiency of nuclear recoil events.

[6] The ^{137}Cs source was found to produce slightly different spectra at different calibration positions. This effect was attributed to spatial non-uniformities in light collection efficiency within the liquid argon volume.

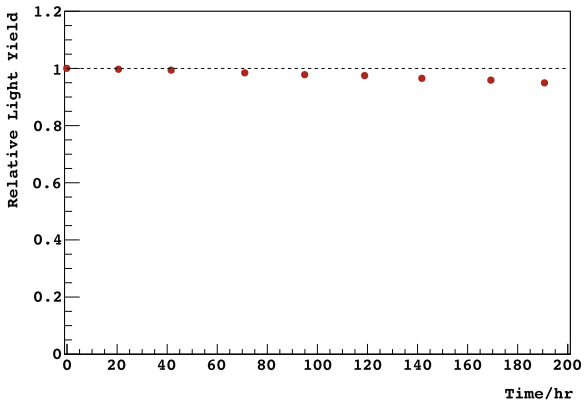

Fig. 4. Relative light yield degradation in the atmospheric argon data measured at KURF; errors are smaller than 1%.

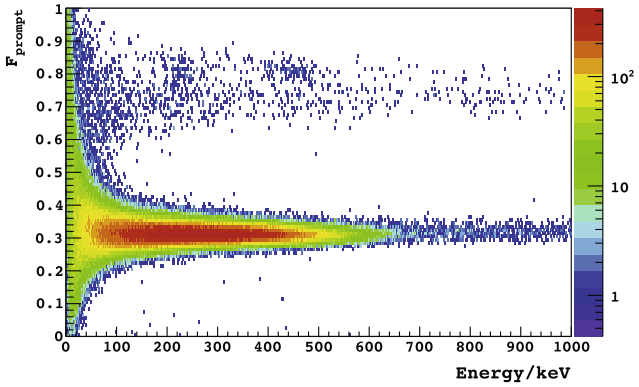

Fig. 5. F_{prompt} vs. energy in the atmospheric argon data measured at KURF. Electron recoil events form the bottom band with F_{prompt} ~0.3, and nuclear recoil events form the top band with F_{prompt} ~0.75.

4.2. Conservative ^{39}Ar analysis

Fig. 6 shows the energy spectra taken with the underground argon during surface commissioning and at KURF. The atmospheric argon spectrum at KURF is also plotted for reference. The muon veto system was able to reduce the background rate by a factor of ~5 at surface, while the underground operation at KURF revealed a background reduction factor of ~25 without the muon veto. The cosmic ray muon rate at KURF was measured, using two of the muon veto panels stacked horizontally, to be ~1 μ/m^2/min, which is approximately 10,000 times lower than that at surface. Due to the low muon rate, the muon veto had no noticeable effect on the underground argon data, and the veto cut was not applied in the analysis to avoid unnecessary dead time. A residual event rate of 20 mBq was observed in the 50–800 keV_{ee} ^{39}Ar window in the measurement of underground argon at KURF.

Data of approximately 100 kg·hr were collected for both underground argon and atmospheric argon at KURF. A conservative upper limit on the ^{39}Ar content in the underground argon was obtained by ignoring the detector background and attributing all of the activity in the underground argon sample to ^{39}Ar. As illustrated in Fig. 7, the ratio of the event rate in underground

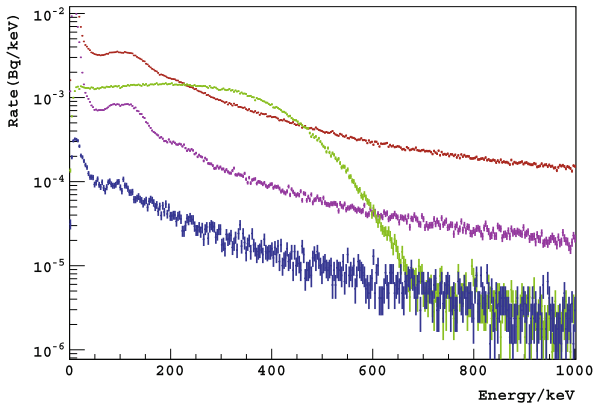

Fig. 6. The energy spectra recorded in the argon detector under different conditions. Red: underground argon data at surface; purple: underground argon data at surface with an active cosmic ray veto; blue: underground argon data at KURF; green: atmospheric argon data at KURF. (For interpretation of the references to color in this figure caption, the reader is referred to the web version of this article.)

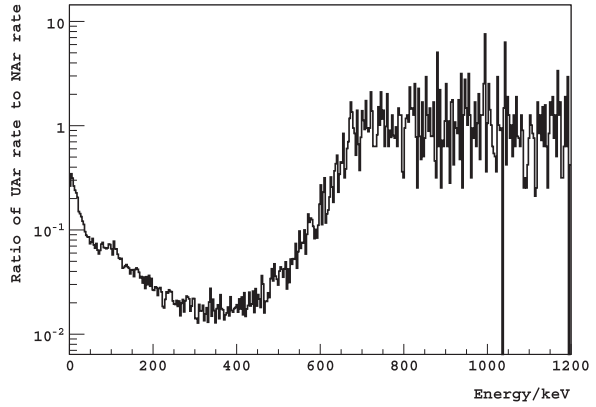

Fig. 7. The ratio of the event rate in underground argon to that in atmospheric argon.

argon to that in atmospheric argon as a function of energy shows that the best energy window to extract an ^{39}Ar upper limit is from 300 keV$_{ee}$ to 400 keV$_{ee}$. The residual event rate in this energy window in the underground argon data after applying the PSD cut was (1.87 ± 0.06) mBq. This is (1.71 ± 0.05)% of the event rate in the atmospheric argon spectrum, and can be taken as a first estimate of the relative ^{39}Ar upper limit in underground argon compared to atmospheric. However, given that background events are included in both spectra and the underground argon data have a lower total rate than the atmospheric data, this estimate must be taken only as a conservative upper limit.

4.3. Background subtraction analysis

A more stringent limit on the abundance of ^{39}Ar in underground argon was obtained by subtracting from the observed underground argon spectrum the estimated events from known background radioactivity. The major background components that were identified were due to the PMT, the PMT base, and the copper shielding. The Geant4 Monte Carlo simulation package [26] was used to estimate the background contribution from these sources. Background contamination from an external source was also identified.

To evaluate the PMT background, three Hamamatsu R11065 PMTs and the electronic components for one PMT base were sent to the Gran Sasso Low Background Counting Facility [27] for radioactivity measurement. As illustrated in Table 1, the U and Th activities were measured at different points of their decay chains. A break in secular equilibrium was identified in the PMT ^{238}U measurement. As a result, the background contribution from the ^{238}U component of the PMT was simulated assuming different activities in the upper part and lower part of the chain. An additional 25% uncertainty was added to the analysis to account for the unknown position of radioactivity inside the PMT.

Table 1
Measured radioactive activity in the major detector components.

Decay chain	Measurement point	PMT (mBq)	Base (mBq)	Cu (mBq/kg)
^{232}Th	^{228}Ra	6 ± 1	41 ± 2.8	–
	^{228}Th	6 ± 1	45 ± 4.7	–
^{238}U	^{234}Th	190 ± 40	25 ± 3.7	–
	^{234m}Pa	90 ± 40	< 149	-
	^{226}Ra	18 ± 1.2	32 ± 1.9	–
^{235}U	^{235}U	7 ± 1	1.4 ± 0.4	–
^{40}K	^{40}K	79 ± 11	65 ± 9.3	–
^{60}Co	^{60}Co	8.8 ± 0.8	< 1.2	2.1 ± 0.19
^{57}Co	^{57}Co	–	–	1.8 ± 0.4
^{58}Co	^{58}Co	–	–	1.7 ± 0.09
^{56}Co	^{56}Co	–	–	0.2 ± 0.03

Background from the cosmogenic radioactivity in the copper shield was also estimated. The specific copper sample in the experiment was not counted; instead, equilibrium cosmogenic copper activation values, as reported in Ref. [28] and as listed in Table 1, were used. The copper measured in the reference was exposed to cosmic rays at LNGS, Italy (altitude 985 m above sea level), and the activities were scaled down by a factor of 2.1 to reflect the lower cosmic ray flux at sea level, as suggested by Ref. [28]. Our Geant4 simulation was used to translate the copper activities into detector background rates. A 25% uncertainty in this background rate was added in the later analysis to account for the uncertainties in the copper exposure history, the variations in the cosmic ray flux with latitude, and the (small) overburdens covering our copper during exposure.

While the backgrounds from the detector materials described above are expected to be identical in the measurements of atmospheric and underground argon, the presence of radioactive noble gas contaminants in the argon could produce a background signal that is different between the two measurements. The radon levels in the measurements were found to be negligible from both alpha studies and ^{214}Bi-^{214}Po coincidence searches. In addition, the observed event rates were stable over time and the two measured energy spectra were consistent above the ^{39}Ar energy window, as illustrated in Fig. 7. Another radioactive nobel gas is ^{85}Kr, an anthropogenic isotope with a beta decay endpoint energy of 687 keV, very close to that of ^{39}Ar. The level of ^{85}Kr in the underground argon is expected to be extremely low because no efficient underground ^{85}Kr production mechanism is known. In any case, ^{85}Kr in the underground argon would be conservatively considered to be ^{39}Ar in the analysis. ^{85}Kr in the atmospheric argon reference sample, on the other hand, could artificially lower the apparent ^{39}Ar activity ratio between the underground and atmospheric argon samples. The krypton level in the high purity atmospheric argon purchased as our standard was measured by the manufacturer to be less than 40 ppb. With a typical ^{85}Kr/Kr ratio of 15 ppt, the ^{85}Kr decay rate in the reference sample would be less than 1.8% of the ^{39}Ar decay rate. A systematic uncertainty was added in the analysis to account for this potential effect.

Besides the intrinsic background in the detector, it was discovered that a weak ^{252}Cf source (~5000 n/s) used by another experiment at KURF contributed non-negligible background to the argon detector, even though it was stored 45 ft away. Removing the ^{252}Cf

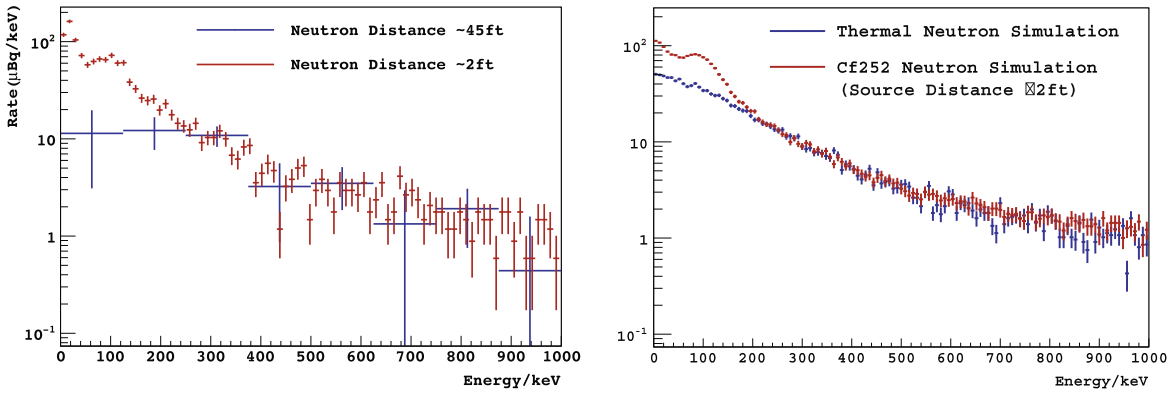

(a) Measured neutron spectra. (b) Simulated neutron spectra.

Fig. 8. (a) the measured energy spectra of electron recoil events induced by the ^{252}Cf neutron source at different distances from the argon detector: ^{252}Cf contamination spectrum (source at 45 ft) and ^{252}Cf calibration spectrum (source at 2 ft); (b) Monte Carlo simulated energy spectra induced by ^{252}Cf neutrons and by thermal neutrons generated right outside the detector shielding. The neutron calibration and simulation spectra have been scaled to match the ^{252}Cf background contamination spectrum above 250 keV$_{ee}$.

source from the lab reduced the underground argon event rate in the 300–400 keV$_{ee}$ window by 40%, but only 3 h of ^{252}Cf-free data were collected because the detector was scheduled to shut down. To investigate this ^{252}Cf background contamination, another short run with the ^{252}Cf source right beside the detector (~2 ft) was taken, which provided a ^{252}Cf neutron source calibration spectrum.

The ^{252}Cf neutron background contamination spectrum (source at 45 ft) is shown in Fig. 8(a), which was produced by subtracting the lifetime-normalized energy spectrum of the ^{252}Cf -free data from the normalized spectrum with the ^{252}Cf source in its storage location. The ^{252}Cf source calibration spectrum (source at 2 ft) is also shown in Fig. 8(a), with its amplitude scaled down to match the ^{252}Cf neutron background spectrum (source at 45 ft). The shapes of the two spectra are similar above 250 keV$_{ee}$, but are significantly different at lower energies.

The low energy difference between the two spectra in Fig. 8(a) is explained by inelastic scattering of fast ^{252}Cf neutrons on ^{19}F nuclei in the PTFE, which produces gamma rays at 110 keV$_{ee}$ and 197 keV$_{ee}$ following the excitation of ^{19}F nuclear energy levels. Signatures of the ^{19}F gamma rays were also observed in the measurements on surface, where high energy cosmogenic neutrons are prevalent, as can be seen in Fig. 6. The suppression of the ^{19}F gammas in the ^{252}Cf neutron background spectrum (source at 45 ft) indicates that the neutrons lose energy before reaching the detector and are less capable of exciting ^{19}F. On the contrary, as discussed below, the energy region above 250 keV$_{ee}$ is dominated by high energy gamma ray emission following the capture of neutrons in different detector components.

Monte Carlo simulations performed using Geant 4.9.6.p03 support the above explanations of the neutron spectra. Fig. 8(b) shows the simulated electron recoil spectra in the low background liquid argon detector induced by ^{252}Cf neutrons and by thermal neutrons generated right outside the detector shielding. Energy resolution equivalent to that in the ^{39}Ar measurement was applied, and the spectra were normalized to match Fig. 8(a) above 250 keV$_{ee}$. The simulations reproduced the low energy features induced by inelastic scattering of ^{252}Cf neutrons on ^{19}F in PTFE. It also confirmed that the spectral shape above 250 keV$_{ee}$ does not depend significantly on the incoming neutron energy, or equivalently, on source position.

To account for the neutron contamination in the bulk of the data, we fitted the ^{252}Cf neutron background spectrum (source at 45 ft) to the ^{252}Cf source calibration spectrum (source at 2 ft) above 250 keV$_{ee}$, and used the fit result and uncertainty to estimate the ^{252}Cf background rate (source at 45 ft) in the energy region of interest. This method includes the uncertainty of the spectral shapes and improves the accuracy of the ^{252}Cf background rate estimation.

Table 2
The expected background rate in 300–400 keV$_{ee}$ from different sources.

Source	^{252}Cf	PMT	Base	Copper
Rate (mBq)	0.82 ± 0.16	0.29 ± 0.08	0.07 ± 0.02	0.36 ± 0.11

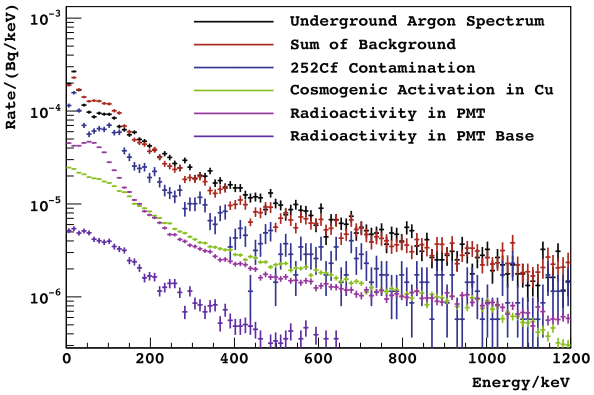

Fig. 9. The background spectra expected from the identified sources of radioactivities compared to the observed spectrum. The rate excess around 100 keV$_{ee}$ in the summed background is due to inelastic neutron scattering in the neutron calibration spectrum.

A summary of the expected background contributions in the 300–400 keV$_{ee}$ energy region of the low background detector measurement is shown in Table 2. To be conservative, the contributions from detector components whose radioactivities were not specifically measured are not included in the background estimation. This includes, for example, the long lived radioisotopes in the OFHC copper shielding, as well as any activity in the PTFE container; at typical radioactivity levels reported by other authors, these contributions would be small.

In addition to the statistical uncertainties in the activity measurements listed in Table 1 and the systematic uncertainties discussed earlier, the PMT and base background estimates in Table 2. include a 25% uncertainty to account for the unknown

Table 3
A summary of the background subtraction analysis. The entire upper limit ^{85}Kr rate is taken as an uncertainty in the background subtracted NAr rate. To convert these rates into activities per unit mass, an argon active mass of 0.56 ± 0.03 kg can be used.

	Rate/mBq, (300, 400) keV
Natural Ar (NAr)	108.78 ± 0.39
Underground Ar (UAr)	1.87 ± 0.06
Estimated background	1.54 ± 0.22
^{85}Kr in NAr	< 1.83
NAr, background subtracted	107.2 ± 1.9
UAr, background subtracted	0.32 ± 0.23

spatial distribution of the radioactive contaminants within the components. Additionally, we include a 5% uncertainty to account for approximations in the Monte Carlo geometry for all radioactivity simulations.

The total predicted background spectrum is shown in Fig. 9, together with the individual spectra from each of the components. The high statistics ^{252}Cf source calibration spectrum is scaled and used in place of the ^{252}Cf background spectrum (source at 45 ft). Above 200–250 keV$_{ee}$, the summed background spectrum looks similar to the observed one; the excess of events around 100–200 keV$_{ee}$ compared to the observed spectrum is due to neutron inelastic scattering in the neutron calibration data, as discussed above.

The known background components account for 80% of the activity in the underground argon spectrum in 300–400 keV$_{ee}$. After subtracting the estimated backgrounds, a residual event rate of (0.32 ± 0.23) mBq remains in that energy region, as summarized in Table 3. From this we deduce a 95% C.L. upper limit of 0.65% on the ^{39}Ar activity in underground argon relative to that in atmospheric argon. Using the reported ^{39}Ar activity of (1.01 ± 0.08) Bq/kg in natural argon [5], we can similarly obtain a 95% C.L. upper limit of 6.6 mBq/kg on the specific ^{39}Ar activity in this underground argon sample.

5. Measurement of the second underground argon sample

The DarkSide-50 detector would be the first dark matter detector utilizing the low ^{39}Ar underground argon as the active volume. To confirm the low ^{39}Ar concentration in the batch processed underground argon [14,20], a sub-kilogram sample (the second sample) was measured for ^{39}Ar radioactivity with the low background detector. This measurement took place in summer 2012 and the difference from the previous measurement is summarized below.

1. The ^{252}Cf source was removed from the underground laboratory.
2. The R11065 PMT was replaced with a lower radioactivity model R11065–10 and the customized high voltage divider was upgraded to low-radioactivity, PTFE-based version utilizing surface-mount components.
3. The high-crystalline Teflon container was replaced with a Spectralon one in the hope of increasing light yield.

Unexpectedly, the event rate in the second sample was found to be higher than that in the 2011 measurement using the first sample, as shown in Fig. 10(left). Because the higher rate was also observed at energy levels above the ^{39}Ar end point, it was not interpreted as an increase of ^{39}Ar content in the second sample. Further analysis of this data showed that the event rate decreased over time, as shown in Fig. 10(right). The gamma/electron event rate between 300 keV$_{ee}$ and 800 keV$_{ee}$ decreased by ~30% over 80 hrs, and the alpha-like event rate dropped by 50%. By contrast, the event rate in the measurement of the first sample was very stable over time. It is suspected that the additional background in the second sample was due to radon contamination although the statistics of the acquired data were not adequate to measure the half life of the rate decay.

A simple rate analysis without background subtraction yielded an upper limit of 2.0% on the ^{39}Ar concentration in the second underground argon sample relative to atmospheric, compared to the 1.8% result from the first sample. If the decreasing background component in the second sample is attributed to radon, and the radon rate inferred from the observed decrease is subtracted, the relative ^{39}Ar upper limit can be brought down to ~1%. Due to the significant uncertainty from the radon contamination, background subtraction analysis was not performed on this sample. We expect the DarkSide-50 detector to provide a more sensitive measurement of the ^{39}Ar activity in this batch of underground argon in its 2015 operation.

6. Mantle origin hypothesis for the underground argon

The extraordinarily low ^{39}Ar content in the underground argon gas extracted from the Doe Canyon field suggests that this argon originates from the Earth's mantle, instead of from the crust where the ^{39}Ar content has been found to be relatively high [6–8]. Further support of this hypothesis can be obtained from the study of stable argon isotope ratios [11–13].

Atmospheric argon has a ratio of ^{40}Ar/^{36}Ar of 295.5 [29], whereas Mid Ocean Ridge Basalts, which were derived by partial melting of the upper mantle, have measured ^{40}Ar/^{36}Ar ratios of 296 to 40,000

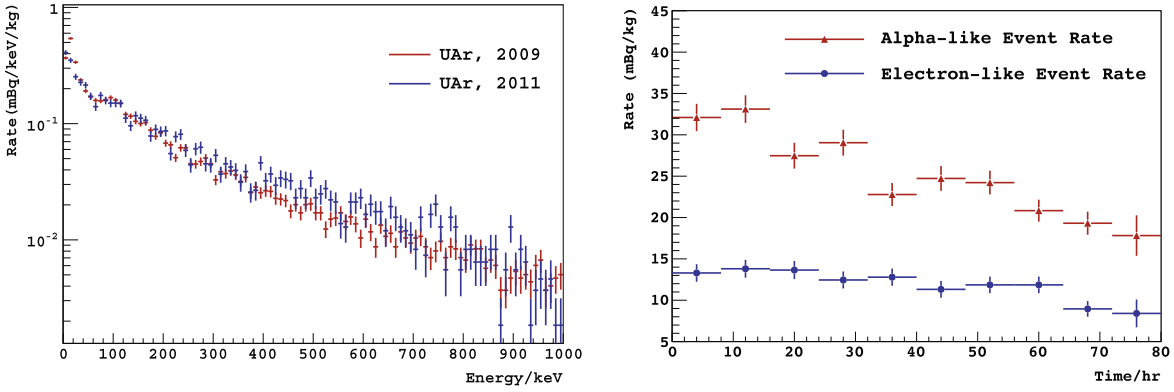

Fig. 10. Left: Mass-normalized energy spectra observed in the first and second underground argon samples. Right: The alpha-like (high F_{prompt}, >1000 keV$_{ee}$) event rate and electron-like (low F_{prompt}, 300–800 keV$_{ee}$) event rate measured in the second underground argon sample.

[30,31]. The large argon isotopic variability in the basalts reflects mixing between the upper mantle argon, which has a $^{40}Ar/^{36}Ar$ value around 41,000, and atmospheric argon introduced into the basalts upon eruption onto the seafloor. By comparison, the $^{40}Ar/^{36}Ar$ ratio for argon from the Doe Canyon CO_2 gas well was measured to be 13,300 using a SRS UGA 300 residual gas analyzer, very close to the mantle values. By contrast, the argon from the National Helium Reserve [9] had a measured $^{40}Ar/^{36}Ar$ ratio of 1,640, which is between atmospheric and mantle values. The low ^{39}Ar limit for the National Helium Reserve compared to expected levels from the crust, and the intermediate value of the $^{40}Ar/^{36}Ar$ ratio may suggest that the source of the gas is deeper than the crust. The argon from the National Helium Reserve was separated from natural gas that is expected to be biotic, and therefore crustal in origin; however, noble gases in crustal fluids can show a mantle signature, particularly in regions that may be undergoing tectonic extension [32]. It should also be noted that there is an alternative hypothesis for a deep origin of natural gas [33].

7. Conclusion

We developed a low background, single phase, liquid argon detector to measure the ^{39}Ar activity in argon obtained from underground sources. The background rate in the detector when operated in the KURF underground laboratory was <4 mHz/kg in the 300–400 keV_{ee} energy range. We obtained an upper limit of 0.65% on the ^{39}Ar activity in the first argon gas sample extracted from the Doe Canyon field in Cortez, Colorado, relative to atmospheric argon, that is, 6.6 mBq/kg specific ^{39}Ar activity. This limit is almost 10 times lower than earlier results [9] and, to the best of our knowledge, demonstrates the highest sensitivity to ^{39}Ar in argon yet obtained. A follow-up measurement using a second underground argon sample confirmed that the ^{39}Ar content has remained low with a similar but slightly higher limit.

This result represents an important milestone in argon-based direct detection dark matter searches, as at this activity multi-ton two-phase detectors can be operated without pileup. The large reduction in ^{39}Ar activity will also allow current and next-generation experiments using underground argon to operate with lower threshold energies than experiments using atmospheric argon. This will improve the sensitivity of argon experiments, especially in the low mass WIMP region. Detailed discussion on the impacts of this work on argon-based rare events detection can be found in [19].

Acknowledgments

We acknowledge the hospitality of the Kimballton Underground Research Facility, and thank the management and staff at Lhoist North America – Kimballton for their valuable support and assistance. We thank Martin Cassidy and Martin Schoell for their invaluable help in identifying suitable sampling locations in New Mexico and Colorado. We thank the management and staff of Kinder Morgan for their support and assistance in hosting us at the Doe Canyon facility in Cortez, Colorado. We gratefully acknowledge the loan of the plastic scintillator muon veto and electronics from Fermi National Accelerator Laboratory and thank Stephen Pordes for his helpful contributions. We thank the Princeton Plasma Physics Laboratory for the use of some additional lead shielding. This work was supported by NSF Grants PHY0704220 and PHY0957083. AW acknowledges support from the Princeton Dicke Fellow program. We acknowledge valuable discussions with, and support from, our colleagues in the DarkSide collaboration.

References

[1] M. Boulay, A. Hime, Astropart. Phys. 25 (2006) 179–182.
[2] C. Jillings, in: Proceeding of the Lake Louise Institute 2008, Fundamental Interactions, pp. 264–268.
[3] M. Boulay et al., 2009. Available from: arXiv:0904.2930.
[4] P. Benetti et al., Astropart. Phys. 28 (2008) 495–507.
[5] P. Benetti et al., Nucl. Instrum. Methods A 574 (2007) 83–88.
[6] H.H. Loosli, B. Lehmann, W. Balderer, Geochim. Cosmochim. Ac. 53 (1989) 1825–1829.
[7] B.E. Lehmann, S.N. Davis, J.T. Fabryka-Martin, Water Resour. Res. 29 (1993) 2027–2040.
[8] H. Loosli, Earth Planet. Sci. Lett. 63 (1983) 51–62.
[9] D. Acosta-Kane et al., Nucl. Instrum. Methods A 587 (2008) 46–51.
[10] T. Lyubetskaya, J. Korenaga, J. Geophys. Res.–Planet. 112 (2007).
[11] T. Staudacher, Nature 325 (1987) 605–607.
[12] M.W. Caffee, G.B. Hudson, C. Velsko, G.R. Huss, E.C. Alexander, A.R. Chivas, Science 285 (1999) 2115–2118.
[13] G. Holland, C.J. Ballentine, Nature (2006) 186–191.
[14] H.O. Back et al., 2012. Available from: arXiv:1204.6024.
[15] P. Collon et al., Nucl. Instrum. Methods B 223–224 (2004) 428–434.
[16] P. Collon et al., Nucl. Instrum. Methods B 283 (2012) 77–83.
[17] W. Jiang et al., Phys. Rev. Lett. 106 (2011).
[18] T. Alexander et al., J. Instrum. 8 (2013).
[19] J. Xu, Study of argon from underground sources for direct dark matter detection (Ph.D. thesis), Princeton University, 2013.
[20] H.O. Back et al. 2012. Available from: arXiv:1204.6061.
[21] J.F. Ziegler, IBM J. Res. Dev. 40 (1996) 19–39.
[22] C. Martoff, P. Lewin, Comput. Phys. Commun. 72 (1992) 96–103.
[23] H. Chu (Senior Thesis), Princeton University, 2010.
[24] C. Lally, G. Davies, W. Jones, N. Smith, Nucl. Instr. Methods Phys. Res. B 117 (1996) 421–427.
[25] D.-M. Mei, Z.-B. Yin, L. Stonehill, A. Hime, Astropart. Phys. 30 (2008) 12–17.
[26] S. Agostinelli et al., Nucl. Instrum. Methods A 506 (2003) 250–303.
[27] C. Arpesella, Appl. Radiat. Isot. 47 (1996) 991–996.
[28] M. Laubenstein, G. Heusser, Appl. Radiat. Isot. 67 (2009) 750–754.
[29] A.O. Nier, Phys. Rev. 77 (1950) 789–793.
[30] P. Sarda, T. Staudacher, C.J. Allgre, Earth Planet. Sci. Lett. 72 (1985) 357–375.
[31] B. Marty, F. Humbert, Earth Planet. Sci. Lett. 152 (1997) 101–112.
[32] R. O'Nions, E. Oxburgh, Earth Planet. Sci. Lett. 90 (1988) 331–347.
[33] T. Gold, F.J. Dyson, The Deep Hot Biosphere: The Myth of Fossil Fuels, Springer, 2001.